Original Article

DOI: 10.5582/ddt.2026.01013

HSD17B12 deficiency is associated with granulosa cell apoptosis and inflammatory transcriptomic signatures in experimental premature ovarian insufficiency models

Xiuxiu Yuan[1,§], Hongjuan Zhao[2,§], Hongli Yan[3,*], Guang Yang[4,*], Yu Wang[3,5,*]

[1] Reproductive Center, Datong Third People's Hospital, Datong, Shanxi, China;
[2] Department of Gynecology and Obstetrics, Shandong Provincial Third Hospital, Shandong University, Jinan, Shandong, China;
[3] Department of Reproductive Medicine, The First Affiliated Hospital of Naval Medical University, Shanghai, China;
[4] Department of General Surgery, Ruijin Hospital, Shanghai Jiao Tong University School of Medicine, Shanghai, China;
[5] Inner Mongolia Medical University affiliated Hospital, Hohhot, China.

SUMMARY: Premature ovarian insufficiency (POI) remains a challenging condition with largely elusive etiology. Granulosa cell (GC) apoptosis is a key event in follicular atresia. This study investigates the correlation between 17β-hydroxysteroid dehydrogenase type 12 (HSD17B12) expression and ovarian dysfunction, specifically examining the transcriptomic landscape associated with *HSD17B12* modulation. A *Tripterygium wilfordii* polyglycoside suspension-induced POI mouse model was established to assess ovarian developmental status and *Hsd17b12* expression. HSD17B12 was overexpressed or knocked down in human granulosa tumor (KGN) and ovarian adenocarcinoma (SKOV3) cell lines. Transcriptomic sequencing was performed to analyze differential gene expression. Both mRNA and protein levels of *Hsd17b12* were significantly downregulated in the ovaries of the POI mouse model. *In vitro*, knockdown of *HSD17B12* suppressed cell proliferation and exacerbated apoptosis in both cell models. Transcriptomic analysis revealed that differentially expressed genes (DEGs) were predominantly enriched in immune regulation and inflammatory response pathways. Specifically, HSD17B12 deficiency led to the significant upregulation of genes involved in the "Cytokine-cytokine receptor interaction" and the "NF-κB signaling pathway". *HSD17B12* regulates proliferation and apoptosis in granulosa-like KGN cells, and *HSD17B12* deficiency is associated with an inflammatory transcriptomic signature in experimental POI models.

Keywords: Premature ovarian insufficiency, *HSD17B12*, granulosa cells, transcriptomics, NF-κB, inflammation

1. Introduction

Premature ovarian insufficiency (POI) is characterized by a reduced ovarian reserve in young women (< 40 years old), with a global prevalence estimated around 1% or higher in specific populations (*1*). Despite advances in genetic diagnosis and biomarker discovery, many POI cases remain idiopathic, underscoring the need to identify novel pathogenic factors and actionable molecular pathways (*2*). Two primary mechanisms are hypothesized to lead to POI: (1) insufficient acquisition of primordial follicles, typically occurring during the fetal period; and (2) excessive activation or accelerated atresia of primordial follicles. These processes lead to the irreversible depletion of the primordial follicle pool, ultimately diminishing follicle number and quality. Early diagnosis and intervention are crucial for POI; however, this remains challenging due to the insidious onset of the disease. Identifying pathogenic genes closely associated with POI progression may reveal potential therapeutic targets and provide a theoretical foundation for disease prevention, early diagnosis, and treatment.

Follicular depletion in POI is closely linked to granulosa cell (GC) dysfunction, where impaired proliferation and excessive apoptosis accelerate follicular atresia (*3,4*). Accumulating evidence also supports a role for ovarian inflammatory signaling in disrupting GC homeostasis. For example, theca-cell-derived IL 1β can act in a paracrine manner to activate NF κB signaling in GCs, increase oxidative stress, suppress steroidogenesis, and ultimately promote GC apoptosis (*5*). Consistently, NF κB-related inflammatory cascades are implicated in immune-mediated POI models and can be therapeutically modulated (*6*).

HSD17B12, a key enzyme catalyzing estrone-to-estradiol conversion, is broadly expressed in the ovary

and has been implicated in female fertility regulation (*7*). Importantly, human genetic and mouse model studies have demonstrated that HSD17B12 dosage insufficiency can directly cause POI and compromise ovarian reserve and fertility (*8*). However, the downstream transcriptomic programs linking *HSD17B12* deficiency to GC injury remain incompletely defined. In the present study, we established a *Tripterygium wilfordii* polyglycoside suspension-induced POI mouse model and manipulated *HSD17B12* expression in KGN cells, with SKOV3 used as a secondary ovarian epithelial context, to investigate its effects on GC survival and to characterize pathway-level changes, with a particular focus on inflammatory and NF-κB--associated signatures.

2. Materials and Methods

2.1. Establishment of the POI mouse model

Thirty-two female C57BL/6 mice (8–10 weeks old; Beijing Vital River Laboratory Animal Technology Co., Ltd.,Beijing,China) were housed in a specific-pathogen-free (SPF) barrier facility (20–24°C, 45%–65% humidity) at Inner Mongolia Medical University. They were provided with a standard diet, purified water, and a 12-hour light-dark cycle. All animal care procedures adhered to the ARRIVE guidelines and were approved by the Animal Ethics Committee of Inner Mongolia Medical University (Approval No. YKD202201213). Vaginal cytology was performed daily at 9:00 AM for 7 consecutive days. Mice with regular estrous cycles were randomly divided into two groups: a control group (n = 16) and a POI group (n = 16). The POI model was established by intragastric administration of a *Tripterygium wilfordii* polyglycoside suspension (Yuanda Medicine Huangshi Feiyun Pharmaceutical Co., Ltd., Huangshi, China.) (80 mg/kg/day) dissolved in 0.9% normal saline for 14 days. General physiological indexes and estrous cycles were monitored daily.

2.2. Tissue collection and processing

Two days post-treatment, mice were weighed, and orbital blood samples were collected. Samples were incubated at 4°C for 1 hour, and serum was obtained by centrifugation at 12,000 rpm for 15 min at 4°C, then stored at -80°C. Mice were sacrificed by cervical dislocation; uteri and ovaries were harvested and weighed. Right ovaries from four mice per group were fixed in 4% paraformaldehyde for histological analysis, while remaining tissues were snap-frozen for molecular studies.

2.3. Organ index, histological analysis, and hormone assay

2.3.1. Morphometric analysis of ovarian and uterine sections

Paraffin-embedded ovarian and uterine tissues were sectioned at 5 μm and stained with hematoxylin and eosin (H&E). Representative sections were imaged under a light microscope, and the cross-sectional areas of the ovary and uterus were measured using ImageJ software. For each animal, the mean area from serial sections was used for statistical analysis (mm^2).

2.3.2. Histological observation and follicle counting

Ovaries were fixed in 4% paraformaldehyde and embedded in paraffin. Serial sections were cut at a thickness of 5 μm. To avoid double-counting, every section was mounted on glass slides, and the first section was discarded. Follicle counting was initiated from the third section and continued every 20 μm throughout the entire ovary. Under a light microscope, follicles were classified and counted as primordial follicles , early growth follicles, and atretic follicles based on their morphological characteristics.

2.3.3. Serum anti-Müllerian hormone (AMH) detection by ELISA

Mouse serum was collected and stored at -80°C. Before analysis, samples were thawed at room temperature and centrifuged at 12,000 × g for 5 min at 4°C to remove debris. The concentration of AMH in the serum was quantified using a commercial ELISA kit according to the manufacturer's instructions (Double-antibody sandwich method).

2.4. Quantitative real-time PCR (qRT-PCR)

Total RNA (1 μg) from each sample was reverse-transcribed into cDNA using a MicroRNA RT Kit (Takara, Kusatsu, Japan). qRT-PCR was performed in triplicate on an ABI Prism 7300HT system using a SYBR Green PCR Kit and gene-specific primers (Takara, Table 1) according to the manufacturer's instructions. Relative mRNA levels were determined using the $2^{-\Delta\Delta Ct}$ method.

2.5. Western blotting

Ovarian tissues were homogenized in RIPA lysis buffer (Beijing Suolaibao Technology Co., Ltd). Equal amounts of protein were separated by 8% SDS-PAGE

Table 1. Primer sequences

Gene	Sequence (5'-3')	Tm (°C)
HSD17B12-Forward	TCTGGAAATTCCCGACTTGGAC	68.14
HSD17B12-Reverse	TCTACCATGCCAGGCAGCAC	68.58
GAPDH- Forward	TGTGTCCGTCGTGGATCTGA	68.10
GAPDH- Reverse	TTGCTGTTGAAGTCGCAGGAG	67.68

(Coolaber) and subsequently transferred to nitrocellulose membranes. The membranes were blocked with 5% non-fat milk in TBST and incubated overnight at 4°C with primary antibodies against HSD17B12 (1:500, BBI Life Sciences Corporation) or GAPDH (1:1,000, Abcam). Following washing, the membranes were incubated with HRP-conjugated goat anti-rabbit or anti-mouse IgG secondary antibodies (1:20,000, Santa Cruz Biotechnology) for 1 h at room temperature. Protein bands were visualized using an enhanced chemiluminescence (ECL) system.

2.6. Cell culture and lentiviral transduction

Human granulosa tumor (KGN) and ovarian adenocarcinoma (SKOV3) cells (Henan Province Engineering Research Center for Applied Microbiology, China) were used. Cells were infected with lentiviral vectors carrying HSD17B12 shRNA, HSD17B12 cDNA, or the corresponding negative control constructs. The HSD17B12 shRNA lentiviral construct was generated using the GV493 vector backbone, and the HSD17B12 overexpression construct was generated by cloning human HSD17B12 cDNA corresponding to NM_016142 into the GV492 vector backbone. Detailed information regarding the shRNA sequence, negative control sequence, overexpression plasmid, primer sequences, construct IDs, and viral titers is provided in Supplementary Table S1 (*https://www.ddtjournal.com/action/getSupplementalData.php?ID=321*).

Lentiviral transduction was performed using HiTransG P reagent for KGN cells and HiTransG A reagent for SKOV3 cells according to the manufacturer's instructions. Cells were seeded at $3 – 5 \times 10^4$ cells/mL (20-30% confluence) and infected at MOI = 100 (KGN) or MOI = 50 (SKOV3). Transduction efficiency (~80%) was verified by fluorescence microscopy 72 h post-infection. Stable cell lines were established and validated *via* qRT-PCR and Western blotting.

2.7. Cell proliferation assay

Cell viability was assessed using the Cell Counting Kit-8 (CCK-8; Dalian Boglin Biotechnology). Transfected cells were seeded in 96-well plates and cultured for 0, 24, 48, and 72 h. At each time point, 10 μL of CCK-8 solution was added, and plates were incubated for 2 h. Absorbance at 450 nm was measured using a microplate reader. Experiments were performed in triplicate.

2.8. Flow cytometry analysis

Cells from each group were collected, washed with PBS (Meilunbio), and resuspended in 1 × binding buffer to a concentration of 1×10^6 cells/mL. Annexin V-PE (5 μL) and 7-AAD (5-10 μL) were added, mixed gently, and incubated at room temperature in the dark for 15 min. The above experiments were repeated three times. For each group, three independent events were captured, totaling 18 events. Apoptosis was then analyzed using flow cytometry (FACSCelesta/BD).

2.9. RNA sequencing and bioinformatics analysis

Total RNA was extracted from six experimental groups (KGN-NC, KGN-sh, KGN-OE, SKOV3-NC, SKOV3-sh, SKOV3-OE; n = 3 per group). Library construction and sequencing (NovaSeq X Plus, PE150) were conducted by Shanghai Majorbio Bio-pharm Biotechnology Co., Ltd. Raw reads were processed with fastp, aligned to the reference genome using HISAT2, and assembled with StringTie. Differential expression analysis was performed using DESeq2. Genes with $|\log_2 FC| \geqq 2$ and FDR < 0.05 were considered significantly differentially expressed (DEGs). Gene Ontology (GO) and Kyoto Encyclopedia of Genes and Genomes (KEGG) enrichment analyses were conducted using Goatools and Python scipy, respectively (Bonferroni-corrected $P < 0.05$).

2.10. Statistical analysis

Data are presented as mean ± SD. Differences between two groups were analyzed using Student's *t*-test or Mann-Whitney *U* test where appropriate. Multiple comparisons were performed using one-way ANOVA followed by Tukey's post-hoc test. A two-tailed $P < 0.05$ was considered statistically significant.

3. Results

3.1. Phenotypic characterization of the POI Mouse Model

Intragastric administration of *Tripterygium wilfordii* polyglycoside suspension successfully induced ovarian dysfunction. Pre-treatment baseline characteristics showed no significant differences between groups. Post-treatment, the POI group exhibited a significant reduction in body weight compared to controls ($P < 0.001$, Table 2). Morphometric analysis revealed a marked decrease in ovarian area in the POI group ($P = 0.005$, Table 3), while uterine area showed a non-significant downward trend ($P = 0.386$, Table 3).

To validate the specific ovarian injury in the context of systemic toxicity, we performed a comprehensive phenotypic characterization of the model. While the model group exhibited significant weight loss compared to the control group, indicative of systemic effects, the ovaries showed specific pathological changes distinct from general toxicity. Histological analysis revealed a significant increase in the atretic follicle ratio ($P = 0.021$) and a decrease in the number of primordial ($P = 0.031$) and early growth follicles ($P = 0.021$) in the model group (Figure 1). Furthermore, serum AMH levels, a specific

marker of ovarian reserve, were significantly reduced (P = 0.002), and vaginal smears indicated disrupted estrous cycles (Figure 2). These findings confirm that the *Tripterygium wilfordii* polyglycoside suspension-induced model successfully recapitulates the specific ovarian dysfunction characteristic of POI, despite the presence of systemic weight loss.

3.2. Downregulation of HSD17B12 in POI ovaries and cell models

Given the critical role of *HSD17B12* in gonadal development, we assessed its expression levels. Both mRNA and protein levels of *Hsd17b12* were significantly downregulated in the ovaries of POI

Table 2. Body weight comparison between control and POI model mice (mean ± SD, *n* = 16)

Group	Control	POI	t/Z	*P*
Before modeling (body weight)	21.663 ± 0.344	21.531 ± 0.367	0.261	0.694
After modeling (body weight)	21.438 ± 0.336	19.069 ± 0.256	-3.663	< 0.001

Table 3. Ovarian and uterine morphometric analysis in control and POI mice (mean ± SD, subgroup for histology, *n* = 4 per group)

Group	Control (mm^2)	POI (mm^2)	t/Z	*P*
After modeling (ovary area)	3.617 ± 0.230	2.434 ± 0.199	-2.836	0.005
After modeling (uterus area)	83.238 ± 4.594	76.886 ± 6.730	0.779	0.386

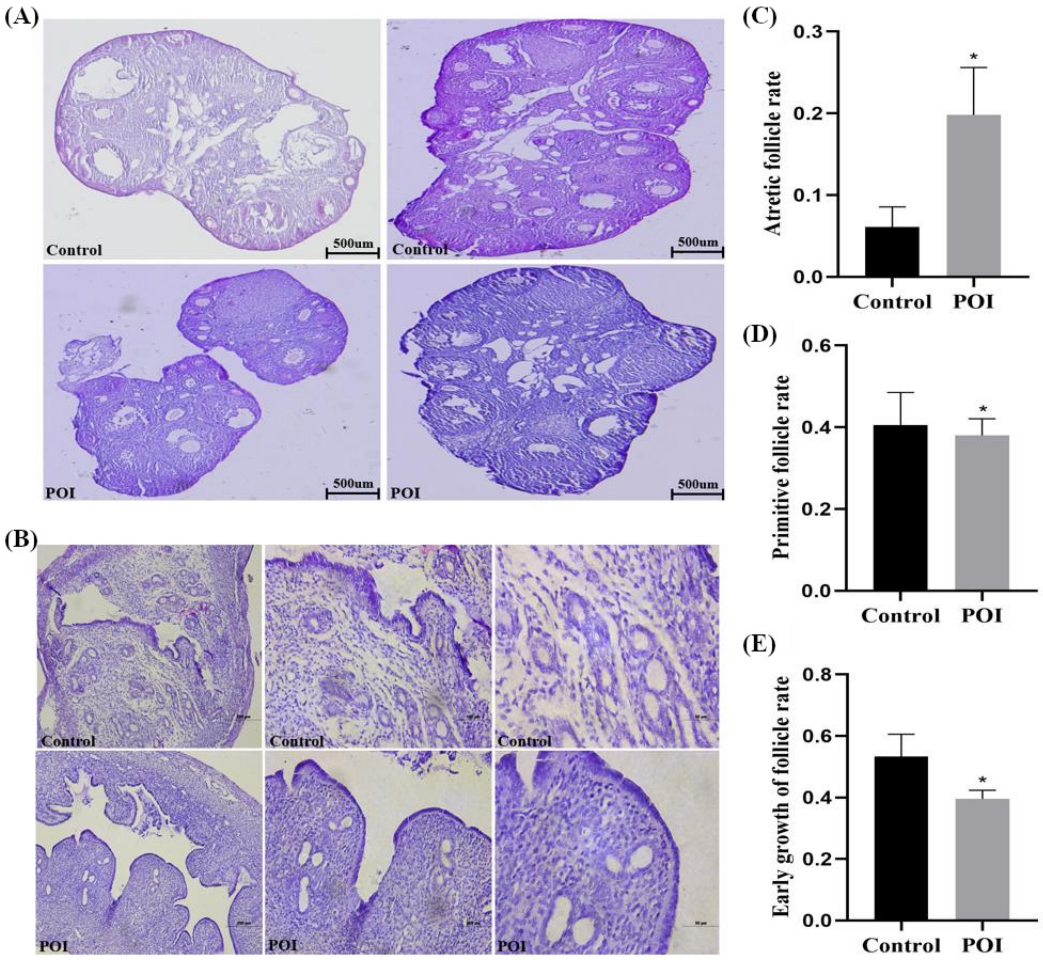


Figure 1. Histopathological analysis and follicle quantification in mouse ovaries. (**A**) Representative H&E staining of whole ovarian sections from Control and POI groups (Scale bar: 500 μm). (**B**) High-magnification views showing follicular morphology (Scale bar: 50 μm). (**C–E**) Quantification of the rates of (**C**) atretic follicles, (**D**) primordial follicles, and (**E**) early growth follicles (primary and secondary) in Control *vs.* POI ovaries (n = 4 mice per group). Data are presented as mean ± SEM. Statistical significance was determined by Student's t-test. *P < 0.05 *vs.* Control group.

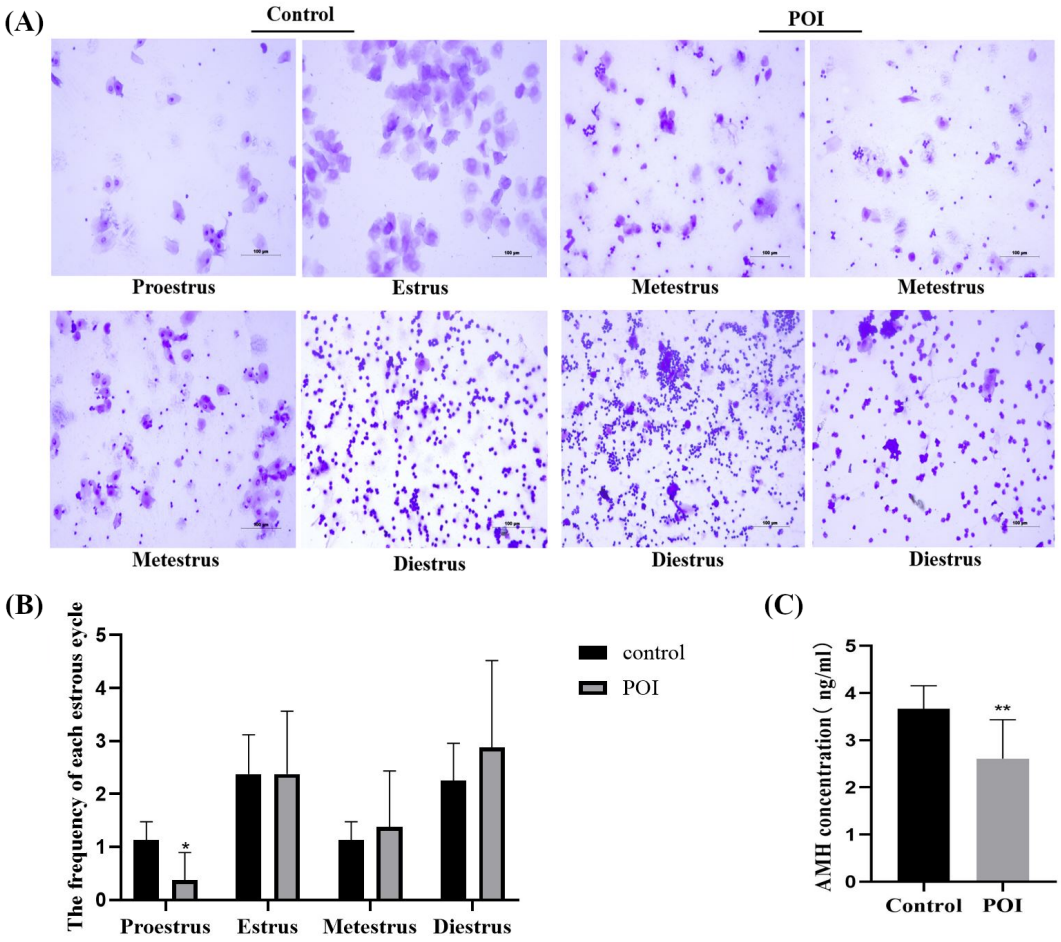


Figure 2. Assessment of estrous-cycle regularity and ovarian reserve function. (**A**) Representative photomicrographs of vaginal cytology at different estrous-cycle stages, including proestrus, estrus, metestrus, and diestrus, in Control and POI mice. Scale bars, 100 μm. (**B**) Statistical analysis of the frequency of each estrous cycle stage over the observation period. Data are presented as mean ± SD (n = 8 mice per group). (**C**) Serum anti-Müllerian hormone (AMH) concentrations in Control and POI mice. Data are presented as mean ± SEM (n = 8 mice per group). Statistical significance was determined using Student's t-test. *P < 0.05 and **P < 0.01 *vs*. Control group.

mice compared to controls (Figure 3). To investigate functional consequences, we modulated *HSD17B12* expression in KGN and SKOV3 cells. Fluorescence microscopy confirmed a transduction efficiency of approximately 80% (Supplementary Figure S1, *https://www.ddtjournal.com/action/getSupplementalData.php?ID=321*). Validation experiments demonstrated successful knockdown and overexpression of *HSD17B12* at both transcriptional and translational levels in stable cell lines (Figure 4). These results confirm that *HSD17B12* expression is significantly compromised in the POI context.

3.3. *HSD17B12* modulates cell proliferation and apoptosis

CCK-8 assays revealed that *HSD17B12* knockdown significantly inhibited proliferation in both KGN and SKOV3 cells at 24, 48, and 72 h, whereas overexpression promoted proliferation compared to respective controls (Figures 5A-B). Flow cytometry analysis indicated that *HSD17B12* knockdown markedly increased the apoptotic rate in KGN cells compared to NC (P = 0.006) and OE groups (P = 0.038); however, overexpression did not significantly reduce apoptosis below baseline levels (P = 0.179, Figure 5C). Similarly, in SKOV3 cells, knockdown induced significant apoptosis (P = 0.009 *vs*. NC; P = 0.034 *vs.* OE), while overexpression showed no significant protective effect against baseline apoptosis (P = 0.724, Figure 5D).

3.4. Transcriptomic profiling reveals immune and inflammatory dysregulation

RNA-seq analysis identified substantial transcriptional alterations upon *HSD17B12* modulation (Supplementary Figure S2, *https://www.ddtjournal.com/action/getSupplementalData.php?ID=321*). In KGN cells, comparison between OE and NC groups yielded 447 DEGs (289 upregulated, 158 downregulated; P < 0.001 , FC > 4.0), while sh *vs.* NC comparison revealed 1,171 DEGs (889 upregulated, 282 downregulated). In SKOV3 cells, 520 DEGs were identified in the OE group and 370 in the sh group (Figure 6).

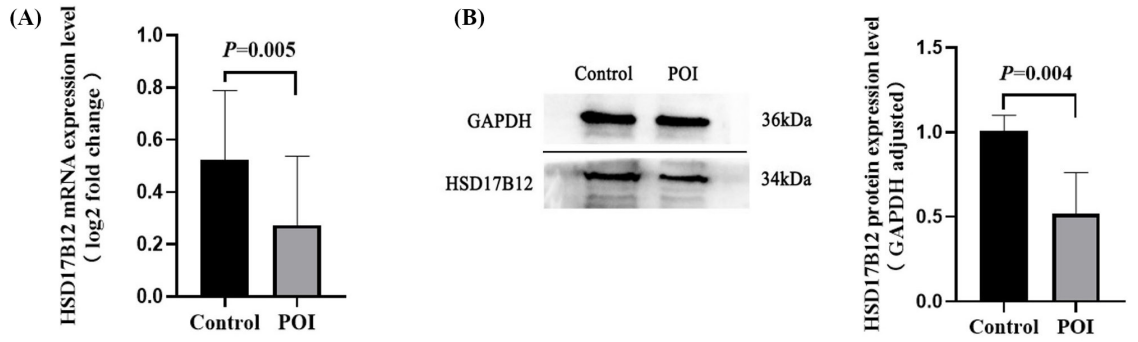


Figure 3. Expression of HSD17B12 in the ovaries of Control and POI mice. (**A**) Quantitative RT-PCR analysis of Hsd17b12 mRNA levels (n = 10 mice per group). (**B**) Representative Western blot image and densitometry quantification of HSD17B12 protein levels (n = 3 independent experiments). Data are presented as mean ± SD. Statistical significance was determined by Student's t-test. Specific P values are indicated in the graphs.

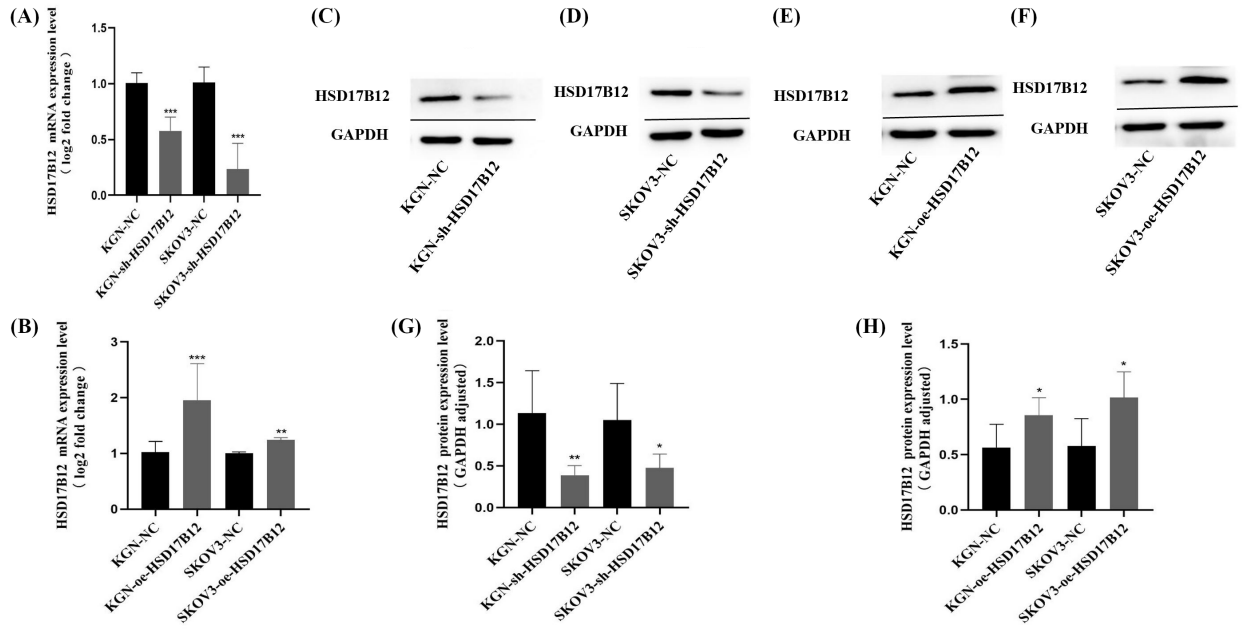


Figure 4. Validation of *HSD17B12* knockdown and overexpression in KGN and SKOV3 cells. (**A-B**) qRT-PCR analysis. (**C-H**) Representative Western blot images and densitometry quantification. Data are presented as mean ± SD from n = 3 independent experiments. Statistical significance was determined by one-way ANOVA followed by Tukey's post hoc test. (*P < 0.05, **P < 0.01, ***P < 0.001).

To delineate the potential mechanism linking HSD17B12 to apoptosis, we focused on the immune and inflammatory pathways. KEGG analysis revealed significant enrichment in "Cytokine-cytokine receptor interaction' and 'NF-κB signaling pathway" (Figure 7). Furthermore, GO analysis highlighted a cluster of terms related to immune response, including MHC class II molecules, von Willebrand factor (vWF), and chemokine activity (Figure 8). Specifically, HSD17B12 knockdown led to the upregulation of key pro-inflammatory genes, suggesting that HSD17B12 deficiency may create a pro-inflammatory transcriptomic landscape that predisposes granulosa cells to apoptosis.

4. Discussion

POI pathogenesis is increasingly linked to aberrant granulosa cell dynamics, including impaired proliferation and excessive apoptosis, leading to follicular atresia. *HSD17B12* encodes a key enzyme in estrogen biosynthesis, converting estrone to the more potent estradiol, thereby regulating oogenesis and ovulation. Prior studies indicate that *Hsd17b12* haploinsufficiency in mice results in subfertility, smaller litter sizes, and meiotic arrest in immature follicles, likely mediated by disrupted arachidonic acid metabolism (*7*). Similarly, in Nile tilapia, *HSD17B12* is implicated in oocyte maturation *via* steroidogenesis (*9*). Consistent with these findings, our study demonstrates significant downregulation of *Hsd17b12* in a *Tripterygium wilfordii* polyglycoside suspension-induced POI mouse model. Functionally, *HSD17B12* overexpression promoted proliferation, whereas knockdown inhibited proliferation and increased apoptosis; however, overexpression did not

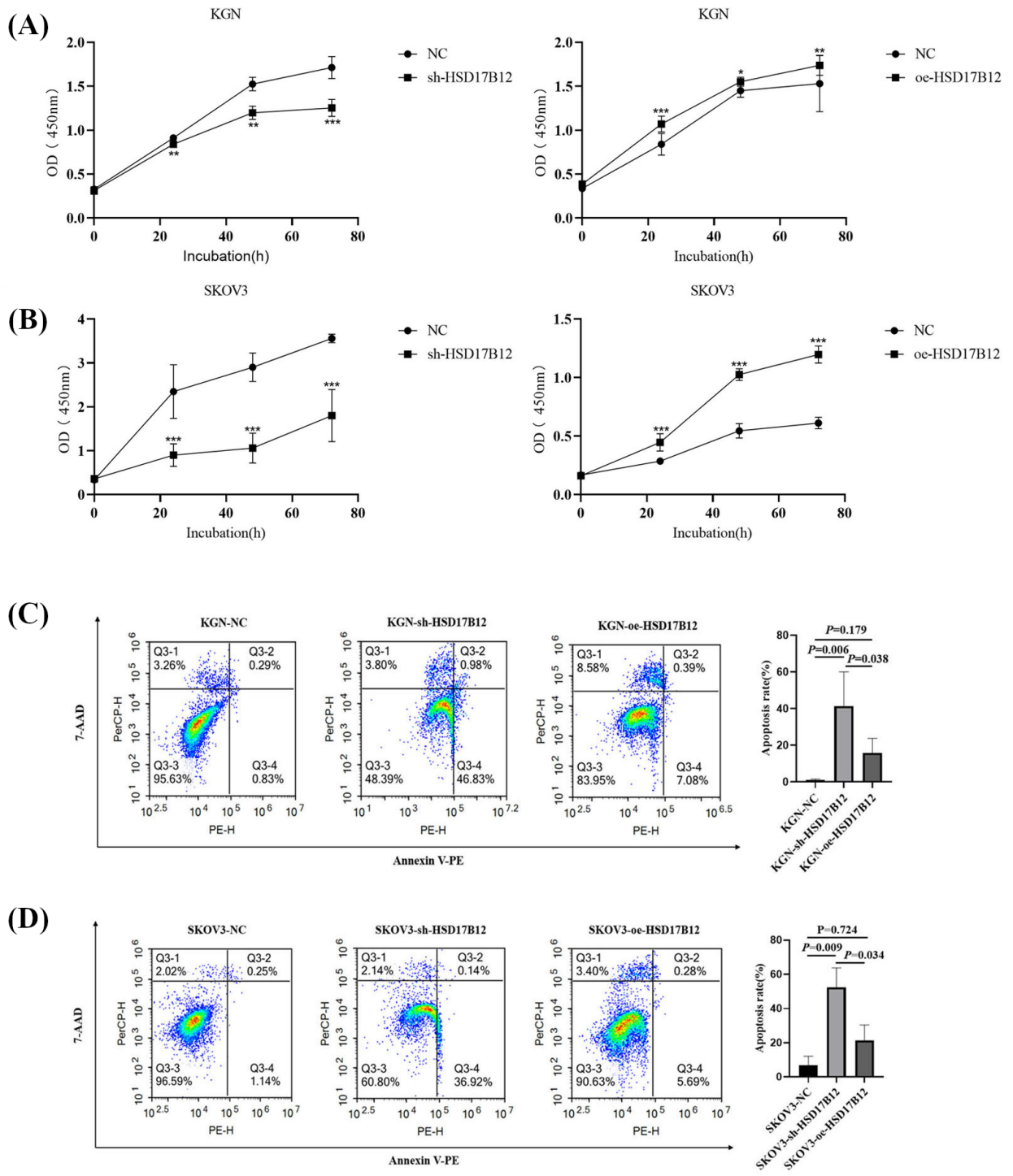


Figure 5. Effects of *HSD17B12* modulation on cell proliferation and apoptosis. (**A-B**) CCK-8 assays in KGN and SKOV3 cells at 0, 24, 48, and 72 h. The 0 h OD values were measured immediately after seeding and were comparable among groups. (**C-D**) Flow cytometric analysis of apoptosis. Data represent mean ± SD ($n = 3$). *$P < 0.05$, **$P < 0.01$, ***$P < 0.001$ (one-way ANOVA with Tukey's test).

significantly reduce apoptosis under our experimental conditions.

Recent studies indicate that POI pathogenesis is closely associated with chronic inflammation. Elevated levels of inflammatory factors and cells in peripheral blood, ovarian tissue, and follicular fluid of POI patients suggest that GCs and oocytes are damaged *via* inflammatory mechanisms. M1 macrophages and their secreted pro-inflammatory cytokines can activate primary follicles, whereas M2 macrophages maintain follicular dormancy (*10*). Sun *et al.* (*11*) reported significantly elevated serum IL-6 and IL-21 levels in patients with primary POI compared with controls. Previous studies have confirmed elevated serum TNF-α, IL-1, and IL-6 levels in POI patients (*12*). Moreover, Acayak *et al.* (*13*) demonstrated that the neutrophil-

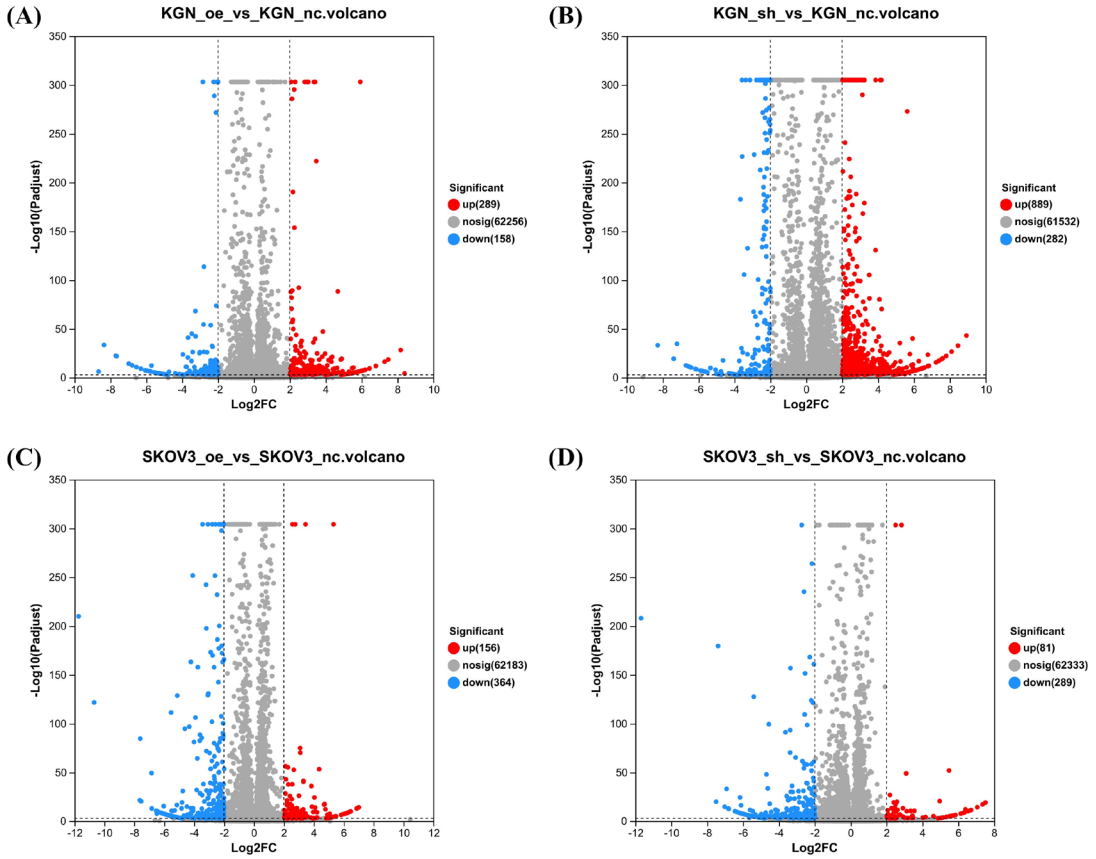


Figure 6. Volcano plots of differentially expressed genes (DEGs). Transcriptomic profiles of (**A**, **B**) KGN cells and (**C**, **D**) SKOV3 cells were analyzed. Comparisons were made between (**A**, **C**) Overexpression (OE) *vs.* Negative Control (NC) and (**B**, **D**) Knockdown (sh) *vs.* NC. Red dots represent significantly upregulated genes, blue dots represent significantly downregulated genes, and gray dots indicate non-significant genes. The screening criteria were set as $|\log_2 FC| \geqq 2$ and FDR < 0.05. The number of DEGs identified in each comparison is annotated in the legend (*e.g.*, 289 upregulated and 158 downregulated genes in KGN-OE *vs.* NC).

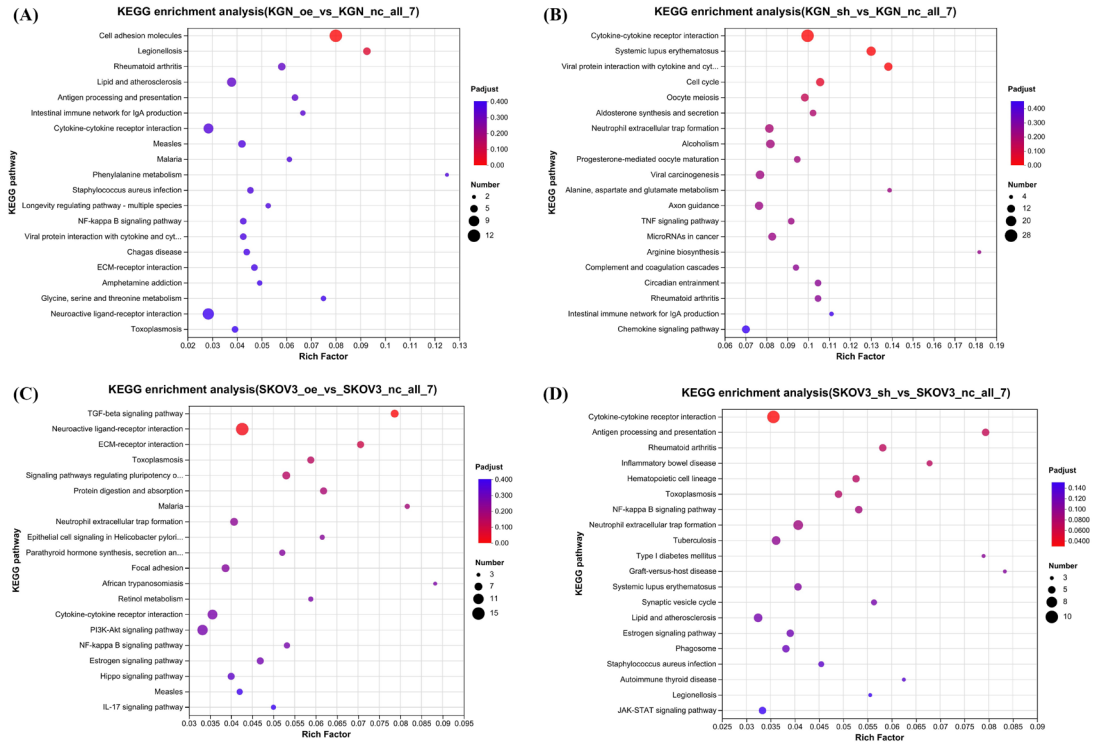


Figure 7. KEGG pathway enrichment analysis of DEGs. Top enriched pathways in KGN (**A, B**) and SKOV3 (**C, D**) cells comparing overexpression (OE) *vs.* negative control (NC) (**A, C**) and knockdown (sh) *vs.* NC (**B, D**). Dot size represents the number of enriched genes, and color intensity (from blue to red) indicates statistical significance (adjusted *P*-value).

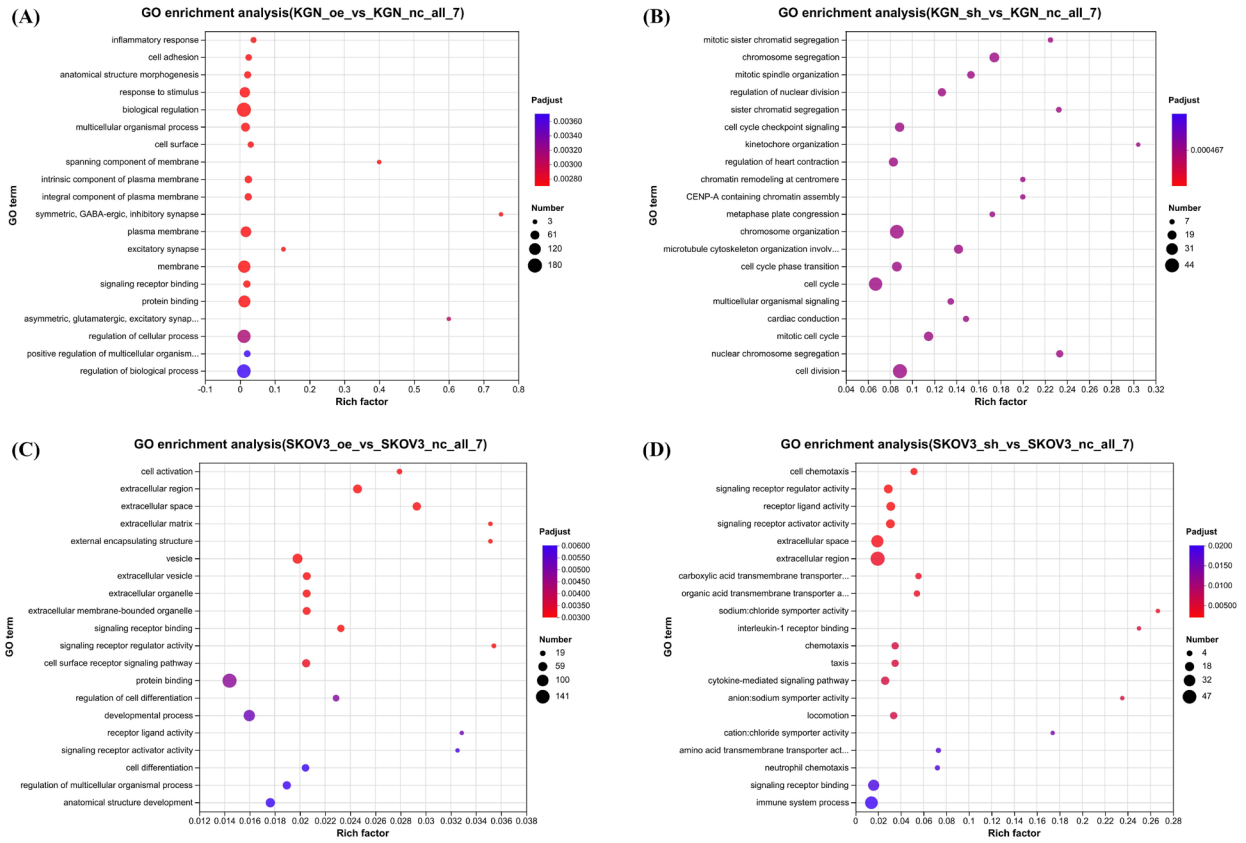


Figure 8. Gene Ontology (GO) biological process enrichment analysis. Top enriched GO terms in KGN (**A**, **B**) and SKOV3 (**C**, **D**) cells comparing overexpression (OE) *vs.* negative control (NC) (**A**, **C**) and knockdown (sh) *vs.* NC (**B**, **D**). Dot size represents the number of enriched genes, and color intensity (from blue to red) indicates statistical significance (adjusted *P*-value).

to-lymphocyte ratio (NLR), an indicator of systemic inflammation, was significantly higher in patients with idiopathic POI than in healthy controls, suggesting a link between inflammation and idiopathic POI. Within follicles, the elevated inflammatory status of GCs is significantly negatively correlated with oocyte quality (*14*). TNF-α in the follicle may upregulate the NF-κB pathway in GCs, increasing IL-1 and IL-6 secretion and thereby reducing oocyte quality. However, the detailed mechanisms by which these inflammatory components promote POI progression remain elusive.

Our transcriptomic data provides a novel perspective by identifying a strong correlation between *HSD17B12* deficiency and the activation of pro-inflammatory pathways. Specifically, in *HSD17B12* knockdown/overexpression cell models, RNA-seq analysis suggests that inflammatory and NF-κB-related pathways may participate in *HSD17B12* deficiency-induced cellular injury. While the precise molecular cascade requires further validation, we propose a novel mechanistic hypothesis (Figure 9): *HSD17B12* deficiency may act as an upstream metabolic trigger, leading to dysregulation of the ovarian immune microenvironment. Specifically, given HSD17B12's role in steroidogenesis and fatty acid metabolism (*15,16*), its downregulation could potentially alter metabolic intermediates that serve as ligands or

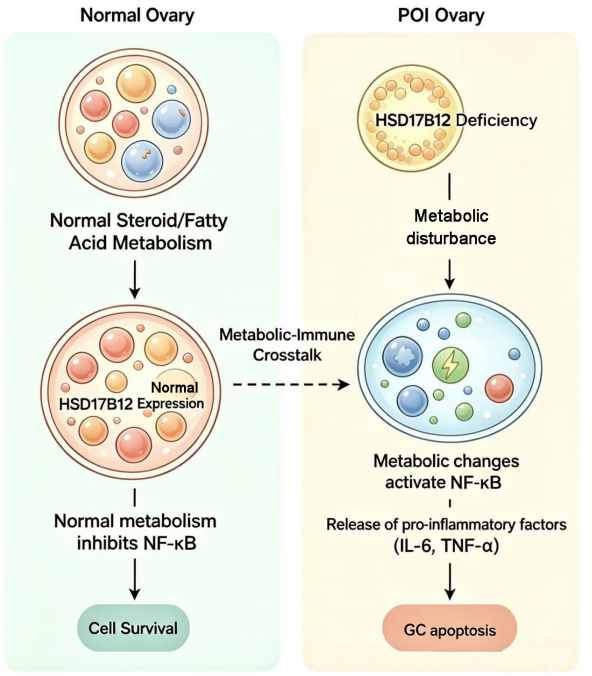


Figure 9. Schematic illustration of the proposed working model. *HSD17B12* deficiency may induce metabolic reprogramming and inflammatory transcriptomic changes, including NF-κB-related signatures, thereby contributing to granulosa cell apoptosis and POI development.

modulators for immune receptors, thereby activating the NF-κB pathway and ultimately inducing granulosa cell apoptosis (*17*).

Several limitations of this study should be acknowledged. First, regarding the model systems, while our chemical-induced mouse model demonstrated specific ovarian damage (evidenced by reduced AMH, disrupted estrous cycles, and follicular atresia), the observed weight loss suggests potential systemic toxicity, which may confound the interpretation of our results. Furthermore, although KGN cells are a well-established model for human granulosa cells, our *in vitro* findings using tumor-derived cell lines cannot fully recapitulate the complexity of primary human ovarian tissue. Second, in terms of research depth, this study represents a transcriptome-guided mechanistic hypothesis. We acknowledge that direct evidence, such as Western blot validation of p-NF-κB or rescue experiments using NF-κB inhibitors, is currently lacking. However, our identification of the "steroid metabolism-immune crosstalk" axis offers a new conceptual framework for understanding POI pathogenesis. Although *HSD17B12* modulation affected proliferation and apoptosis in both KGN and SKOV3 cells, KGN is the primary granulosa-like model, whereas SKOV3 is an ovarian cancer-derived epithelial context; therefore, the granulosa-cell relevance of our findings should be interpreted mainly on the basis of the KGN data. Despite these limitations, our study provides compelling evidence linking HSD17B12 deficiency to granulosa cell apoptosis and inflammatory dysregulation. Future studies involving patient samples and *in vivo* mechanistic interventions are necessary to fully delineate the therapeutic potential of targeting HSD17B12 in POI.

5. Conclusion

HSD17B12 expression is significantly altered in the ovaries of POI mice, directly affecting the proliferation and apoptosis of human ovarian cells. Furthermore, our findings suggest that HSD17B12 contributes to POI pathogenesis by modulating immune and inflammatory response pathways, highlighting a potential "steroid metabolism-immune crosstalk" axis. Future studies involving patient samples and *in vivo* mechanistic interventions are necessary to fully delineate the therapeutic potential of targeting HSD17B12 in POI.

Funding: This work was supported by a grant from the Inner Mongolia Grassland Talents Innovation Team Project (2022), Translational medicine project of Inner Mongolia Medical University, Inner Mongolia Medical University doctoral program construction unit fund matching project (RC2300002962), Inner Mongolia Autonomous Region Science and Technology Plan Project, granted by Inner Mongolia Reproductive Health Research Center (2022YFSH0067,2023KJHZ0038), Inner Mongolia Academy of Medical Sciences public hospital research joint fund project (2024GLLH0368) and Shandong Province Medical and Health Science and Technology Project (202405010322).

Conflict of Interest: The authors have no conflicts of interest to disclose.

References

1. Golezar S, Ramezani Tehrani F, Khazaei S, Ebadi A, Keshavarz Z. The global prevalence of primary ovarian insufficiency and early menopause: a meta-analysis. Climacteric. 2019; 22:403-411.
2. He X, Chang X, Zhuang S, Liu J, Wang Y, Qin Y, Guo T. Genome-wide DNA methylation profile and predictive biomarkers in premature ovarian insufficiency. J Genet Genomics. 2025; 52:596-599.
3. Zhao F, Yan L, Zhao X, Wu J, Fang Y, Xin Z, Wang H, Yang X. Aberrantly High FBXO31 Impairs Oocyte Quality in Premature Ovarian Insufficiency. Aging Dis. 2024; 15:804-823.
4. Shao T, Ke H, Liu R, Xu L, Han S, Zhang X, Dang Y, Jiao X, Li W, Chen ZJ, Qin Y, Zhao S. Autophagy regulates differentiation of ovarian granulosa cells through degradation of WT1. Autophagy. 2022; 18:1864-1878.
5. Cao M, Yuan C, Chen X, He G, Chen T, Zong J, Shen C, Wang N, Zhao Y, Zhang B, Li C, Zhou X. METTL3 deficiency leads to ovarian insufficiency due to IL-1beta overexpression in theca cells. Free Radic Biol Med. 2024; 222:72-84.
6. Xie J, Yang Y, Zhuo A, Gao M, Tang L, Xiao Y, Zhu H, Fu X. Exosomes derived from mesenchymal stem cells attenuate NLRP3-related pyroptosis in autoimmune premature ovarian insufficiency *via* the NF-kappaB pathway. Reprod Biomed Online. 2024; 48:103814.
7. Kemilainen H, Adam M, Maki-Jouppila J, Damdimopoulou P, Damdimopoulos AE, Kere J, Hovatta O, Laajala TD, Aittokallio T, Adamski J, Ryberg H, Ohlsson C, Strauss L, Poutanen M. The Hydroxysteroid (17beta) Dehydrogenase Family Gene HSD17B12 Is Involved in the Prostaglandin Synthesis Pathway, the Ovarian Function, and Regulation of Fertility. Endocrinology. 2016; 157:3719-3730.
8. Wang Q, Chen Q, Zhang Y, *et al*. HSD17B12 dosage insufficiency induced premature ovarian insufficiency in humans and mice. Clin Transl Med. 2022; 12:e737.
9. Aranyakanont C, Ijiri S, Hasegawa Y, Adachi S. 17beta-Hydroxysteroid dehydrogenase type 12 is responsible for maturation-inducing steroid synthesis during oocyte maturation in Nile tilapia. Gen Comp Endocrinol. 2020; 290:113399.
10. Xiao Y, Peng X, Peng Y, Zhang C, Liu W, Yang W, Dou X, Jiang Y, Wang Y, Yang S, Xiang W, Wu T, Li J. Macrophage-derived extracellular vesicles regulate follicular activation and improve ovarian function in old mice by modulating local environment. Clin Transl Med. 2022; 12:e1071.
11. Sun S, Chen H, Zheng X, Ma C, Yue R. Analysis on the level of IL-6, IL-21, AMH in patients with auto-immunity premature ovarian failure and study of correlation. Exp Ther Med. 2018; 16:3395-3398.
12. Vital Reyes VS, Tellez Velasco S, Hinojosa Cruz JC, Ortiz Romero Mde J, Chavarria Olarte ME, Reyes Fuentes A.

Serum levels of IL-1beta, IL-6 and TNF-alpha in infertile patients with ovarian dysfunction. Ginecol Obstet Mex. 2005; 73:604-610.
13. Agacayak E, Yaman Goruk N, Kusen H, Yaman Tunc S, Basaranoglu S, Icen MS, Yildizbakan A, Yuksel H, Kalkanli S, Gul T. Role of inflammation and oxidative stress in the etiology of primary ovarian insufficiency. Turk J Obstet Gynecol. 2016; 13:109-115.
14. Chen Y, Xu Y, Lu Y, Li W, Tao F, Zhao Y. Mechanisms of inflammation in premature ovarian insufficiency and advances in therapeutic studies. Front Immunol. 2026; 17:1765073.
15. Lawrence BM, O'Donnell L, Gannon AL, Skerrett-Byrne DA, Parameswaran S, Abbott I, Smith S, Handelsman DJ, Rebourcet D, Smith LB. Functional Analysis of HSD17B3-Deficient Male Mice Reveals Roles for HSD17B7 and HSD17B12 in Testosterone Biosynthesis. Endocrinology. 2025; 166.
16. Jeanne F, Pilet S, Bernay B, Lagadu S, Delepee R, Dufour S, Sourdaine P. Characterization of a direct role of GnRHs in the control of spermiogenesis and steroidogenesis in the small-spotted catshark Scyliorhinus canicula. Gen Comp Endocrinol. 2025; 368:114734.
17. Hu N, Gao Y, Fan R, Xue Y, Fang S, Wu S, Luo T, Hu L, Zhang D, Zheng L. Eriodictyol mitigates polystyrene nanoplastic-induced ovarian toxicity *via* targeted inhibition of the TLR4/NF-kappaB/NLRP3 inflammatory axis. Environ Pollut. 2026; 397:128007.

Received March 3, 2026; Revised June 18, 2026; Re-revised September 3, 2026; Accepted September 20, 2026.

[§]These authors contributed equally to this work.

**Address correspondence to:*

Hongli Yan, Department of Reproductive Medicine, The First Affiliated Hospital of Naval Medical University, No. 168 Changhai Road, Yangpu District, Shanghai, China.
E-mail: 499166624@qq.com

Guang Yang, Department of General Surgery, Ruijin Hospital, Shanghai Jiao Tong University School of Medicine, No. 197 Ruijin Second Road, Shanghai, China.
E-mail: aguangsun@sina.com

Yu Wang, Department of Reproductive Medicine, The First Affiliated Hospital of Naval Medical University, No. 168 Changhai Road, Yangpu District, Shanghai, China.
E-mail: wuai1544@163.com

Released online in J-STAGE as advance publication October 29, 2026.